Geophys. J. Int. (2001) **147,** 330–342

Rupture propagation beyond fault discontinuities: significance of fault strike and location

Yuko Kase[1,*] and Keiko Kuge[2]

[1] *Disaster Prevention Research Institute, Kyoto University, Gokasho, Uji, Kyoto* 611-0011, *Japan*
[2] *Department of Geophysics, Kyoto University, Kyoto* 606-8502, *Japan*

Accepted 2001 June 6. Received 2001 May 31; in original form 2000 October 24

SUMMARY

Earthquake rupture sometimes occurs on several faults, and often decelerates or terminates at fault stepovers. Factors that control the rupture processes across stepovers are important for an understanding of earthquake growth and termination. In this study, we investigate such factors by calculating the spontaneous rupture processes of two non-coplanar faults in a 3-D model. Dealing with two extreme models in which two strike-slip faults are either parallel or perpendicular, we show that the rupture processes beyond fault discontinuities are drastically different for the two models. We find three factors influencing rupture processes beyond fault discontinuities: depth of the upper edge of the two faults, location of the edge of the first fault and geometry of the two faults. These factors determine the time and location of rupture jumps to the second fault. For rupture propagation to the second fault, it is essential for rupture on the first fault to arrive at the edge of the fault. In particular, whether rupture on the first fault reaches the Earth's surface or not controls the difficulty of rupture jumps and the locations where the rupture is triggered, which is also related to the step direction of the two faults. This is because the stress perturbation at the fault edge is affected by the Earth's free surface.

Key words: cracks, fault models, fractures, rupture propagation.

1 INTRODUCTION

Earthquake faults are often segmented. In some cases, rupture jumps from one subfault to another, but in some cases, rupture decelerates and terminates at fault discontinuities such as jogs and stepovers (e.g. Aki 1979; Lindh & Boore 1981; Sibson 1985, 1986; Scholz 1990). The 1992 Landers earthquake is a typical instance of earthquakes occurring on several subfaults. The rupture propagated across a few kilometres of extensional jogs, and became an M_w7.3 event (Fig. 1) (e.g. Wald & Heaton 1994; Aydin & Du 1995). The rupture of the 1998 Antarctic earthquake (M_w8.1) is composed of two predominant subfaults (e.g. Nettles *et al.* 1999; Kuge *et al.* 1999; Henry *et al.* 2000). Antonioli *et al.* (2000) suggested that the dynamic stress change caused by the first subevent triggered the second over a 70–100 km unbroken barrier. The May event of the 1997 Kagoshima earthquake (M_w6.0) occurred on two conjugate faults (Fig. 2) (Miyamachi *et al.* 1999). The time lag of the ruptures on the two subfaults was between 1 and 2 s (Miyake *et al.* 1999; Horikawa 2001). Whether a rupture can jump beyond the fault discontinuities or not is important for earthquake growth and termination, and this affects the earthquake's size. While distributions of initial stress, strength and stress drop on faults are likely to affect rupture propagation beyond the fault discontinuities, there has also been interest in the role of fault geometry (e.g. King & Nábělek 1985).

The effect of fault geometry on rupture propagation has been studied in relation to the interaction of faults. In studies considering the dynamic interaction of faults, Yamashita & Umeda (1994) and Kame & Yamashita (1997) showed that interaction between faults can cause a deceleration of dynamic rupture. Harris *et al.* (1991) and Harris & Day (1993) showed that the geometry of fault jogs, as defined by Scholz (1990), can determine the distance and location of a rupture jump at a stepover. Spontaneous rupture propagation on two non-coplanar in-plane faults was examined by Kase & Kuge (1998) using two extreme models in which two faults were either parallel or perpendicular. They found that the rupture process triggered on the second fault depends on the strike and location of the two faults. The studies mentioned above are based

* Now at: Active Fault Research Center, National Institute of Advanced Industrial Science and Technology, Tsukuba, Japan. E-mail: kasep@ni.aist.go.jp

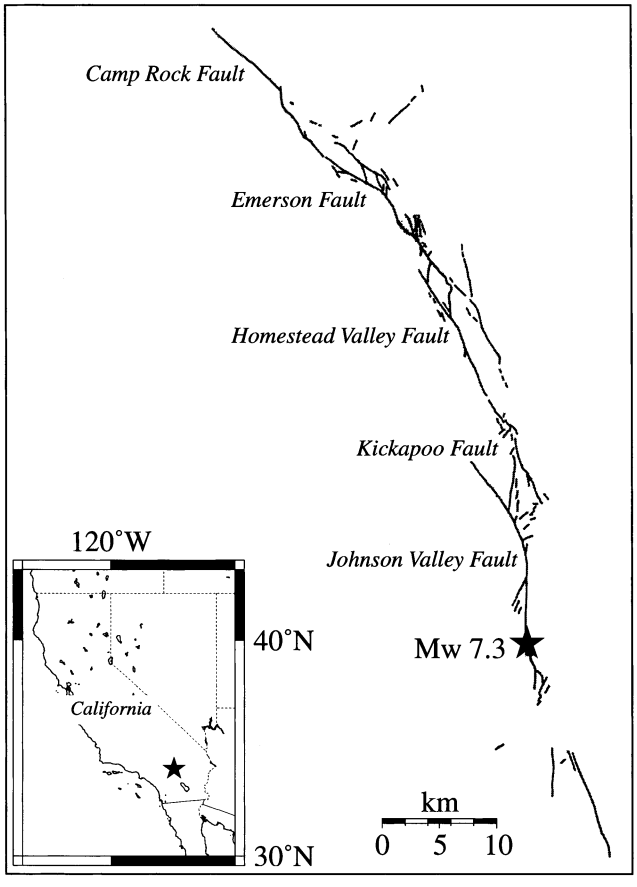

Figure 1. Surface rupture in the 1992 Landers earthquake. Simplified from Hart *et al.* (1993).

on 2-D calculations. For 3-D calculations, Magistrale & Day (1999) simulated rupture processes on thrust-fault segments with tear faults. Harris & Day (1999) obtained results for a segmented strike-slip faults model that were similar to their 2-D simulations (Harris *et al.* 1991; Harris & Day 1993).

The Earth's surface is a very distinctive boundary in the stress/displacement field of the elastic Earth, and should play a significant role in the rupture processes of faults (e.g. Mikumo *et al.* 1987). However, the effect of the Earth's surface on rupture propagation across fault discontinuities has been investigated in only a few studies because 3-D simulations are required. Although Harris & Day (1999) performed 3-D simulations, they did not explain the effect of the Earth's surface in detail.

The purpose of this study is to explore factors that influence rupture processes at fault discontinuities. We carry out 3-D numerical simulations of spontaneous rupture processes for two non-coplanar faults, including the interaction between the faults. Following Kase & Kuge (1998), we deal with two extreme models in which two strike-slip faults are either parallel or perpendicular. Wishing to consider the effect of the Earth's surface in detail, we carefully examine the significance of fault strike and location by performing a number of simulations. We show that rupture propagation beyond fault discontinuities is drastically different for the two extreme models. We also show that whether faults intersect with the Earth's surface or not controls the degree of difficulty and the location of the rupture jump beyond the fault discontinuities, depending on the strike and location of faults.

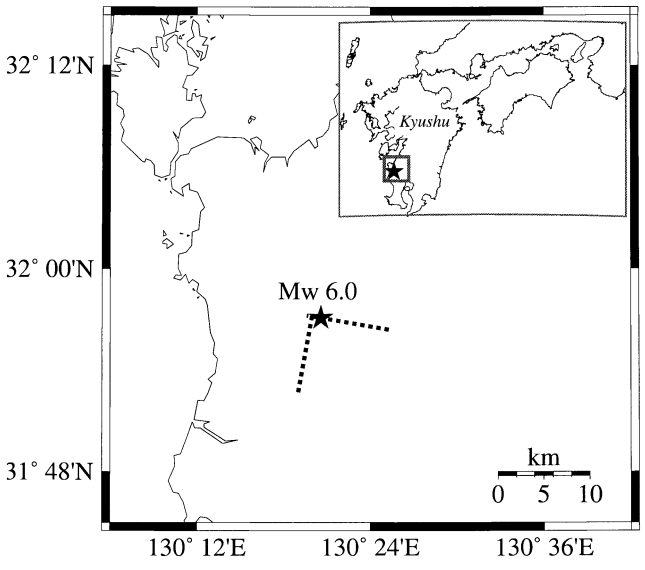

Figure 2. Fault model of the May event of the 1997 Kagoshima earthquake used by Horikawa (2001). The model was based on the aftershock distribution of Miyamachi *et al.* (1999).

2 SIMULATION METHOD

2.1 Models

We put two vertical faults in a 3-D, semi-infinite, homogeneous, isotropic and linear elastic medium (Fig. 3). The medium is subjected to uniform pre-stresses σ_{XX} and σ_{YY}. The first fault (Fault 1) with an initial crack is located on the xz-plane in the medium, where the x- and y-coordinates are oriented at 45° clockwise with respect to the X- and Y-coordinates. Along with Fault 1, we locate a second fault (Fault 2) in the medium, which is either of two fault orientation types. For one type of fault orientation (model A), Fault 2 is parallel to Fault 1. For the other type (model B), Fault 2 is perpendicular to Fault 1, that is, it is parallel to the yz-plane. Rupture can occur only on these two faults, which are weak planes.

At time $t=0$, the shear stress on the initial crack of Fault 1 drops to dynamic frictional stress. The rupture then begins to propagate spontaneously on Fault 1. The rupture causes stress perturbation in the medium, which triggers rupture on Fault 2. Slip occurs on points where shear stress exceeds the static frictional stress, which is equal to the static coefficient of friction times the normal stress. Then, after slip starts, the shear stress obeys the slip-weakening friction law (Fig. 4) (Andrews 1976; Day 1982) and drops to the dynamic frictional stress, which is equal to the dynamic coefficient of friction times the normal stress. We define rupture time as the time when shear stress drops to dynamic frictional stress.

2.2 Equations

Displacements u_x, u_y and u_z at any point satisfy the wave equations

$$\rho\ddot{u}_i = \tau_{ij,j}$$
$$= (\lambda+\mu)u_{j,ji} + \mu u_{i,jj}\,, \qquad (1)$$

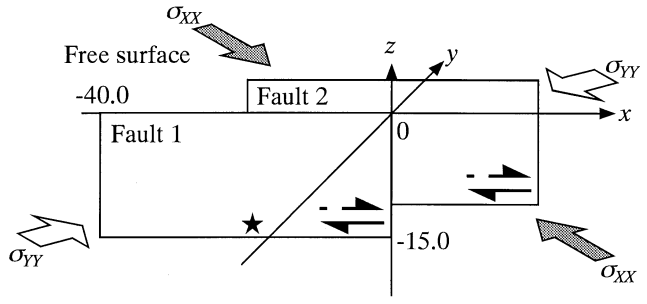

(a) Model A

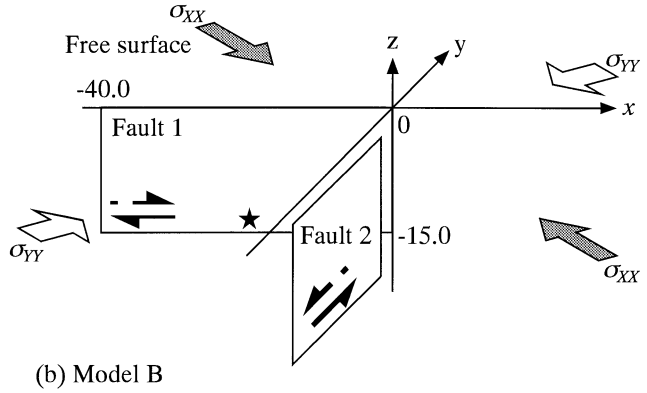

(b) Model B

Figure 3. 3-D models used in this study. Stars indicate the initial cracks. (a) Geometry of two faults in model A (case of compressional jog). Width of two faults is 15.0 km and length is 40.0 km. (b) Geometry of two faults in model B. Two faults are perpendicular to each other. Width of two faults is 15.0 km, and lengths of Fault 1 and 2 are 40.0 and 19.0 km, respectively.

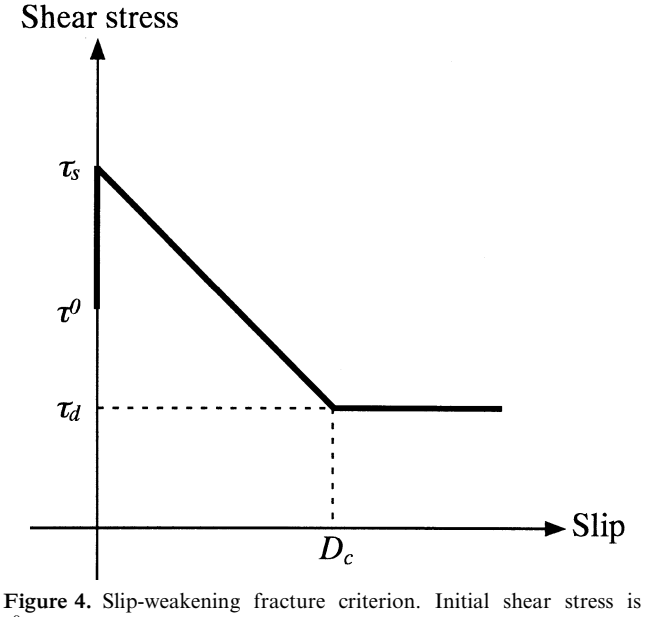

Figure 4. Slip-weakening fracture criterion. Initial shear stress is τ^0. Slip begins when shear stress reaches the static frictional stress, $\tau_s = \mu_s \tau_{normal}$. Shear stress linearly decreases to the dynamic frictional stress, $\tau_d = \mu_d \tau_{normal}$. After slip reaches the critical distance, D_c, shear stress at that point is equal to the dynamic frictional stress.

where ρ is density, and λ and μ are Lame's elastic constants of the medium.

The initial conditions ($t=0$) are

$$u_x = u_y = u_z = 0\,, \tag{2a}$$

$$\frac{\partial u_x}{\partial t} = \frac{\partial u_y}{\partial t} = \frac{\partial u_z}{\partial t} = 0 \tag{2b}$$

at any point. Normal and shear stresses on Fault 1 ($y=0$) are

$$\tau^0_{yy} = \frac{1}{2}\sigma_{XX} + \frac{1}{2}\sigma_{YY}\,, \tag{3a}$$

$$\tau^0_{xy} = \begin{cases} \mu_d \tau^0_{yy} & \text{(on the initial crack)} \\ -\dfrac{1}{2}\sigma_{XX} + \dfrac{1}{2}\sigma_{YY} & \text{(on the others)} \end{cases}, \tag{3b}$$

$$\tau^0_{zy} = 0\,, \tag{3c}$$

where μ_d is the dynamic coefficient of friction. On Fault 2, normal and shear stresses are given by

$$\tau^0_{yy} = \frac{1}{2}\sigma_{XX} + \frac{1}{2}\sigma_{YY}\,, \tag{4a}$$

$$\tau^0_{xy} = -\frac{1}{2}\sigma_{XX} + \frac{1}{2}\sigma_{YY}\,, \tag{4b}$$

$$\tau^0_{zy} = 0 \tag{4c}$$

for model A and

$$\tau^0_{xx} = \tau^0_{yy} = \frac{1}{2}\sigma_{XX} + \frac{1}{2}\sigma_{YY}\,, \tag{5a}$$

$$\tau^0_{yx} = \tau^0_{xy} = -\frac{1}{2}\sigma_{XX} + \frac{1}{2}\sigma_{YY}\,, \tag{5b}$$

$$\tau^0_{zx} = 0 \tag{5c}$$

for model B.

The boundary conditions on Fault 1 and Fault 2 of model A are

$$u_x = \text{continuous}\,, \tag{6a}$$

$$u_y = \text{continuous}\,, \tag{6b}$$

$$u_z = \text{continuous}\,, \tag{6c}$$

$$\tau_{xy} = \tau^0_{xy} + \mu\frac{\partial u_x}{\partial y} + \mu\frac{\partial u_y}{\partial x} = \text{continuous}\,, \tag{6d}$$

$$\tau_{yy} = \tau^0_{yy} + \lambda\frac{\partial u_x}{\partial x} + (\lambda+2\mu)\frac{\partial u_y}{\partial y} + \lambda\frac{\partial u_z}{\partial z} = \text{continuous}\,, \tag{6e}$$

$$\tau_{zy} = \tau^0_{zy} + \mu\frac{\partial u_y}{\partial z} + \mu\frac{\partial u_z}{\partial y} = \text{continuous} \tag{6f}$$

across the fault plane for the region where shear stress has not reached static frictional stress.

For the region where slip has occurred, the boundary conditions are the equations (6b), (6c), (6e) and (6f) and the slip-weakening law (Fig. 4)

$$\tau_{xy} = \begin{cases} \mu_s \tau_{yy} - \dfrac{\mu_s \tau_{yy} - \mu_d \tau_{yy}}{D_c}\Delta u_x = \text{continuous} & \\ \qquad\qquad (\Delta u_x < D_c) & \\ \mu_d \tau_{yy} = \text{continuous} \qquad (\Delta u_x \geq D_c) & \end{cases} \tag{6g}$$

across the fault plane, where μ_s is the static coefficient of friction, D_c is critical displacement and Δu_x is slip.

On Fault 2 of model B, the boundary conditions are

$$u_x = \text{continuous}, \tag{7a}$$

$$u_y = \text{continuous}, \tag{7b}$$

$$u_z = \text{continuous}, \tag{7c}$$

$$\tau_{xx} = \tau^0_{xx} + (\lambda + 2\mu)\frac{\partial u_x}{\partial x} + \lambda\frac{\partial u_y}{\partial y} + \lambda\frac{\partial u_z}{\partial z} = \text{continuous}, \tag{7d}$$

$$\tau_{yx} = \tau_{xy} = \text{continuous}, \tag{7e}$$

$$\tau_{zx} = \tau^0_{zx} + \mu\frac{\partial u_z}{\partial x} + \mu\frac{\partial u_x}{\partial z} = \text{continuous} \tag{7f}$$

across the fault plane for the region where shear stress has not reached static frictional stress.

For the region where slip has occurred, the boundary conditions are the equations (7a), (7c), (7d) and (7f) and

$$\tau_{yx} = \begin{cases} \mu_s\tau_{xx} - \dfrac{\mu_s\tau_{xx} - \mu_d\tau_{xx}}{D_c}\Delta u_y = \text{continuous} \\ \qquad\qquad\qquad\qquad (\Delta u_y < D_c) \\ \mu_d\tau_{xx} = \text{continuous} \qquad (\Delta u_y \geq D_c) \end{cases} \tag{7g}$$

across the fault plane, where Δu_y is slip.

We calculate displacements by a finite difference method. The wave equation (1) is replaced by the central second-order finite difference equations. On the edges of the model space, displacements are obtained from the absorbing boundary condition (Higdon 1991). We use the formulation of Ilan & Loewenthal (1976) for boundary conditions on the free surface and the formulation of Horikawa (1996) for boundary conditions on faults. In Horikawa's formulation, derivatives of stress with respect to the fault-normal coordinate in the eqs (6d), (6e), (6f), (6g), (7d), (7e), (7f) and (7g) are replaced by the derivatives with respect to the fault-parallel coordinate and time, using the wave equation (1) and Taylor expansion. The resultant derivatives are then rewritten using the finite difference scheme. The equations obtained can be solved explicitly with the conditions for displacement.

2.3 Parameters

Table 1 shows the parameters used in our numerical simulations. We assume that the static and dynamic coefficients of friction and the ratio of strength to stress drop, that is, the S-value (Andrews 1976; Das & Aki 1977),

$$S = \frac{\tau_s - \tau^0}{\tau^0 - \tau_d}, \tag{8}$$

are the same on the two faults.

3 RESULTS

We carried out many numerical simulations, varying the depths of the upper edges of the two faults as well as the relative locations of the two faults. In the simulations in which we observed successful rupture propagation from Fault 1 to Fault 2, rupture was triggered on Fault 2 about 1 s after the rupture on Fault 1 arrived at the fault edge. The growth of the rupture on Fault 1 causes a stress perturbation around the rupture front. While the rupture propagates on Fault 1, the stress perturbation is too small to trigger rupture on Fault 2. After the rupture reaches the edge of Fault 1, the stress perturbation rapidly increases with time, and can finally trigger rupture on Fault 2. Thus, for rupture propagation to Fault 2, it is essential for the rupture on Fault 1 to arrive at the edge of the fault, as observed by Harris & Day (1999).

Table 1. Simulation parameters.

Maximum compressional stress: σ_{XX} [MPa]	65.0
Minimum compressional stress: σ_{YY} [MPa]	25.0
Initial shear stress: τ^0_{xy} [MPa]	20.0
Initial normal stress: τ^0_{xx}, τ^0_{yy} [MPa]	45.0
S	1.86
P-wave velocity [km s^{-1}]	4.6
S-wave velocity [km s^{-1}]	2.66
Density: ρ [g cm^{-3}]	2.5
Critical displacement: D_c [m]	0.10
Static coefficient of friction: μ_s	0.9
Dynamic coefficient of friction: μ_d	0.2
Grid length in space [km]	0.5
Grid length in time [s]	0.05

Our results for model A show that rupture jumps to Fault 2 only when the upper edges of the two faults are very close to or at the Earth's surface. As a result of rupture on Fault 1 intersecting with the Earth's surface, rupture on Fault 2 was triggered at the Earth's surface near the upper-right corner of Fault 1 (Fig. 5), as is obtained by Harris & Day (1999). The triggered rupture was located ahead of the edge of Fault 1 in compressional cases (Fig. 5b) and behind the edge in extensional cases (Fig. 5c). This is similar to a 2-D example from Harris & Day (1993). The time lag for rupture jump is longer in compressional cases than in extensional cases. This disagrees with the results of the 3-D simulations in Harris & Day (1999) but agrees with one of the high S-value (eq. 8) cases of the 2-D simulations in Harris & Day (1993). On the other hand, when the upper edge of Fault 1 was beneath the Earth's surface, rupture could be triggered at the upper edge of Fault 2 (Fig. 6a). On Fault 2 far from Fault 1, rupture was not triggered until the rupture on Fault 1 arrived at the upper-right edge of Fault 1 (Fig. 6b), whether or not Fault 1 reached the Earth's surface. Whether or not the rupture on Fault 1 reaches the Earth's surface and the distance between the two faults determine the location where rupture jumps to Fault 2.

In model B, the relative locations of the two faults are very important to whether rupture can jump or not. In a region where the normal stress generated by rupture on Fault 1 is compressional, rupture never jumps to Fault 2, even if the strength of Fault 2 is much less than that of Fault 1. In a region characterized by extensional normal stress, rupture can jump to Fault 2 when Fault 2 is located close to the edge of Fault 1 (Fig. 7). The depth of the rupture jump drastically varies, depending on the location of Fault 2. It is especially important to note that rupture can jump at a deep depth.

Fig. 8 shows the relationship between the depth of the rupture jump and the horizontal location of Fault 2. Faults 1 and 2 reach the Earth's surface. When Fault 2 is located at the edge of Fault 1 ($x = 0$ km; Fig. 7b), rupture jumps to Fault 2 at the deep depth of 7 km. The rupture on Fault 2 starts to propagate after the rupture on Fault 1 terminates completely

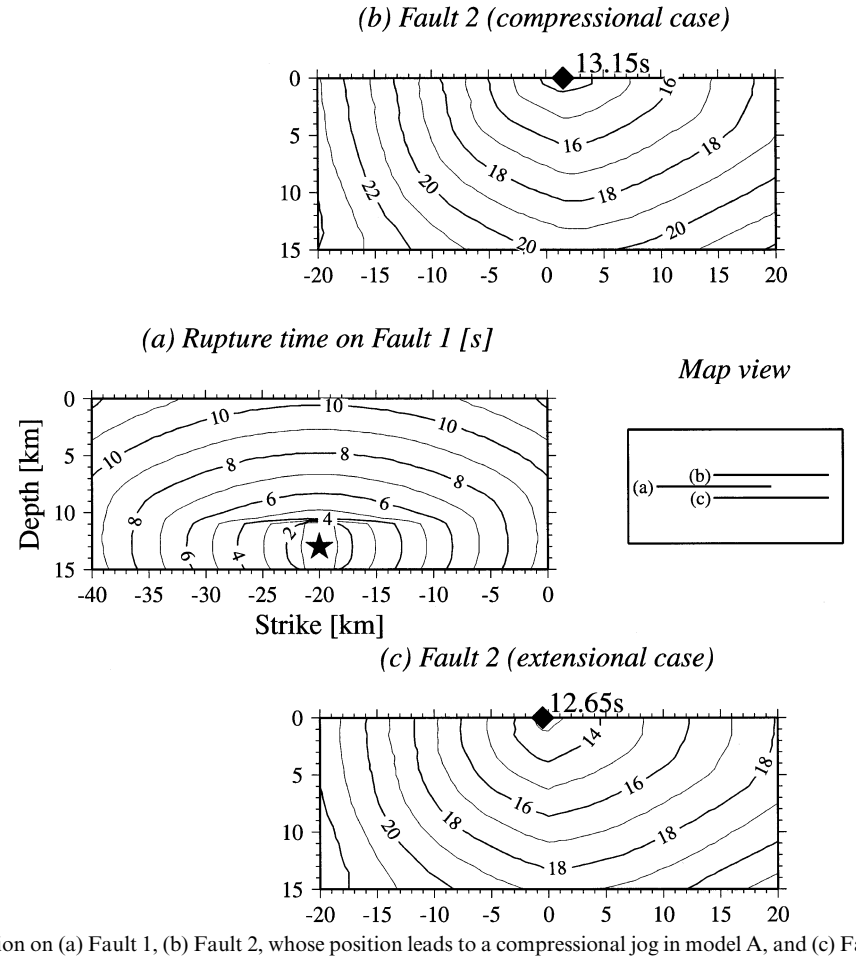

Figure 5. Rupture evolution on (a) Fault 1, (b) Fault 2, whose position leads to a compressional jog in model A, and (c) Fault 2, whose position leads to an extensional jog in model A. Faults 1 and 2 have the same strength and stress drop. Both reach the Earth's surface. Distance between Faults 1 and 2 is 1.0 km. Contours indicate rupture times in seconds. The star is the location of the initial crack. The diamonds are the locations where ruptures are triggered on Fault 2.

(Fig. 7b). In the 2-D simulations of Kase & Kuge (1998), termination of rupture on Fault 1 was not necessary for rupture on Fault 2 to be triggered. The cause of this disagreement is the difference in the values of strength used: the strength of Fault 2 was less than that of Fault 1 in Kase & Kuge (1998), while the strength of the two faults is the same in this study. When Fault 2 is located near the edge of Fault 1 ($x = \pm 2$ km; Figs 7a and c), rupture jumps at the shallow part and propagates. When Fault 2 is located more than 2 km behind the edge of Fault 1, rupture cannot propagate. The distance at which rupture can jump is longer in front of the edge of Fault 1 ($x > 0$) than behind it ($x < 0$). This feature is consistent with Kase & Kuge (1998).

Fig. 9 shows the relationship when Fault 1 is beneath the Earth's surface but when a weak plane of Fault 2 reaches the Earth's surface. When Fault 2 is located at $x = -4$ to -3 km, the rupture is triggered at the Earth's surface. In this region, we did not observe successful rupture jumps when Fault 1 reaches the Earth's surface. When Fault 2 is located far from the edge of Fault 1, rupture cannot be triggered, or can be triggered but soon terminates (see the cross and triangle in Fig. 9). Rupture jumps at deep portions (see $x = -1$ to $+2$ km in Fig. 9) do not depend on whether Fault 1 reaches the Earth's surface or not.

Therefore, our results reveal that the relative location and strike of the two faults are very important not only for whether or not rupture can jump but also for rupture processes, including locations and depths of rupture jumps. It is also remarkable that whether faults reach the Earth's surface or not affects the rupture processes.

4 DISCUSSION

4.1 Effect of the Earth's surface

We have shown that rupture jumps tend to occur at the Earth's surface and that the horizontal location of the rupture jump depends on whether the faults reach the Earth's surface or not. We first discuss the role of the Earth's surface on the rupture jumps, paying particular attention to model A.

The dominant factor affecting rupture jumps is normal stress rather than shear stress. Normal stress on Fault 2 decreases efficiently near the Earth's surface. Therefore, rupture can easily jump at a very shallow depth near the Earth's surface. However, when the rupture on Fault 1 reaches the Earth's surface, the shear stress concentration caused by the rupture is suppressed by dislocation at the free surface. As a result of the insufficient shear stress concentration, rupture on Fault 2 is not triggered until the rupture on Fault 1 arrives at the upper-right edge of Fault 1 and the stress increases near the Earth's surface again (Figs 5b and c).

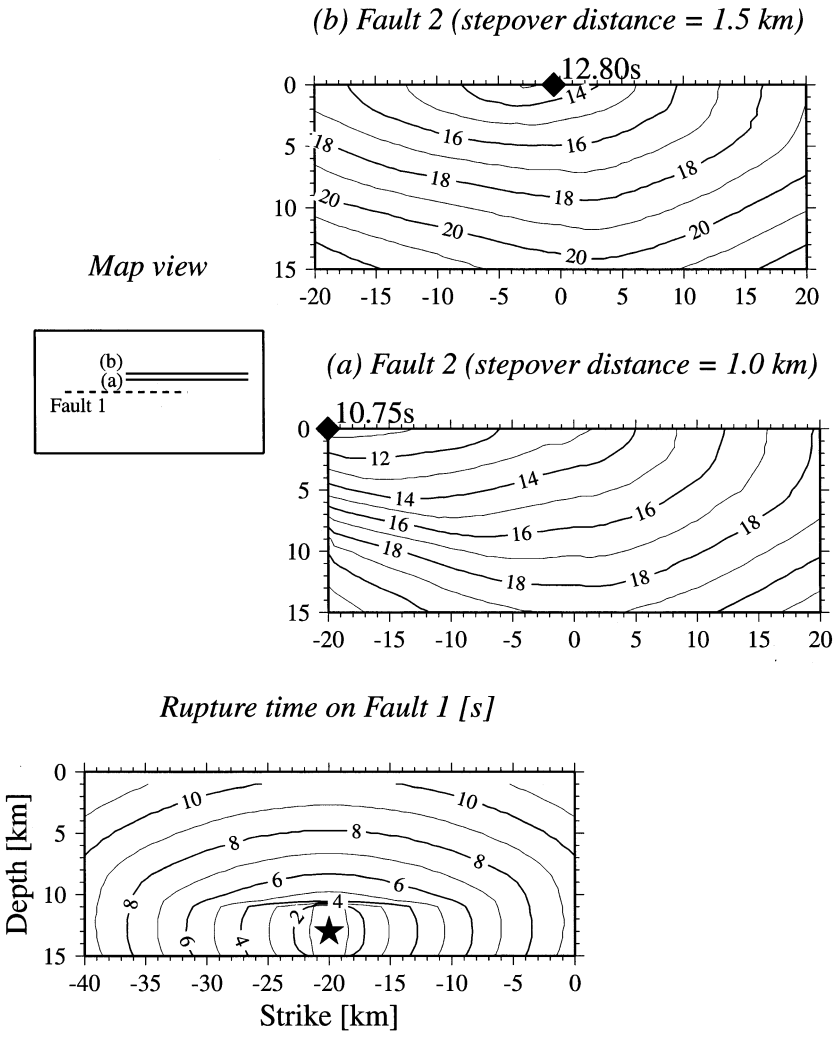

Figure 6. Rupture evolution on Faults 1 and 2 (compressional jog) in model A when Fault 1 does not reach the Earth's surface. The depth of the upper edge of Fault 1 is 1 km. Faults 1 and 2 have the same strength and stress drop as those in Fig. 5. The distance between Faults 1 and 2 is (a) 1.0 km and (b) 1.5 km. The details are the same as for Fig. 5.

When the rupture on Fault 1 terminates beneath the Earth's surface, the shear stress concentration around the upper edge of Fault 1 is significant. If the distance between the two faults is short, the high stress concentration can cause rupture on Fault 2 (Fig. 6a and $x = -4$, -3 km in Fig. 9). As the distance is increased, the influence of the stress concentration on shear stress on Fault 2 becomes small. Rupture is not triggered on Fault 2 at a long distance until the rupture on Fault 1 arrives at the upper-right edge of Fault 1 (Fig. 6b).

Our explanation above is supported by the spatio-temporal distribution of stress difference, which is defined by

$$\Delta s(\boldsymbol{x}, t) = \mu_s|\tau^0_{yy} + \tau_{yy}| - |\tau^0_{xy} + \tau_{xy}| \tag{9a}$$

for model A, and

$$\Delta s(\boldsymbol{x}, t) = \mu_s|\tau^0_{xx} + \tau_{xx}| - |\tau^0_{yx} + \tau_{yx}| \tag{9b}$$

for model B (Harris & Day 1993), where $\boldsymbol{x}$ is position and t is time. Figs 10(a) and 11(a) show the distributions of $\Delta s(\boldsymbol{x}, t)$ for model A when Fault 1 reaches the Earth's surface. A positive $\Delta s(\boldsymbol{x}, t)$ value means that the segment cannot begin to rupture, whereas a negative value means that the segment can initiate rupture. Negative values of $\Delta s(\boldsymbol{x}, t)$ appear around the edge of Fault 1. In particular, beneath the Earth's surface (Fig. 11a), the negative $\Delta s(\boldsymbol{x}, t)$ value is limited to a very small region at the extension of Fault 1. Rupture on Fault 2 is thus triggered only on the Earth's surface around the upper-right edge of Fault 1. Fig. 12(a) shows a case in which rupture on Fault 1 terminates beneath the Earth's surface. $\Delta s(\boldsymbol{x}, t)$ is negative in the large region along the upper edge of Fault 1, indicating that rupture can be triggered there. Therefore, the Earth's surface can affect rupture processes, including locations of rupture jumps, as mentioned above.

The effect of the surface intersection of the rupture on Fault 1 also appears in a discrepancy in rupture propagation between compressional and extensional jogs in model A. Table 2 shows the maximum distance that rupture could jump in our simulations. When the rupture of Fault 1 reaches the Earth's surface, the maximum distance is longer in an extensional jog than in a compressional jog, which agrees with the 2-D result of Harris & Day (1993). When rupture on Fault 1 reaches the Earth's

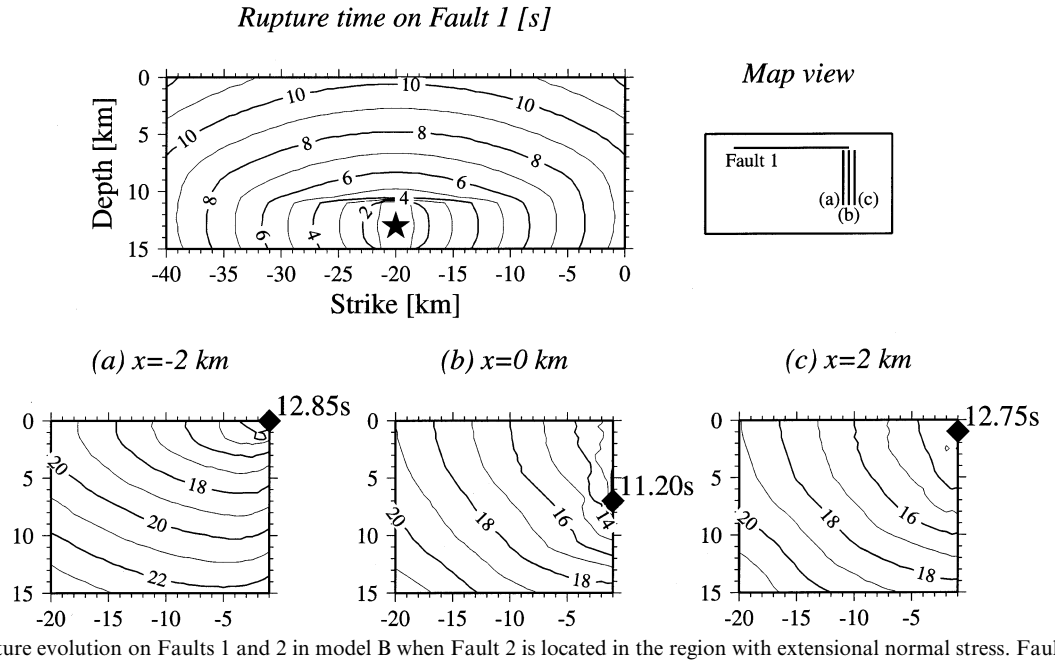

Figure 7. Rupture evolution on Faults 1 and 2 in model B when Fault 2 is located in the region with extensional normal stress. Fault 2 is located at $-20.0\ \text{km} \le y \le -1.0\ \text{km}$ and (a) $x = -2.0$ km, (b) $x = 0$ km and (c) $x = 2.0$ km. Faults 1 and 2 reach the Earth's surface. The details are the same as for Fig. 5.

Table 2. The maximum distance (in kilometres) that rupture can jump.

Depth of upper edge of Fault 1 [km]	Compressional jog	Extensional jog
0.0	1.0	2.0
1.0	2.0	1.5

surface, normal stress, τ_{yy}, on the Earth's surface decreases in an extensional jog, but increases in a compressional jog. The rupture in an extensional jog can, therefore, jump to Fault 2 more easily than when Fault 1 is embedded beneath the Earth's surface (Table 2). In a compressional jog, however, rupture jumps become more difficult.

Rupture abruptly terminated at a fault edge in this study. In real earthquakes, it is also possible that rupture gradually decelerates, for example, as a result of a small or negative stress drop at a shallower depth (e.g. Quin 1990; Harris & Day 1999). Further discussion is necessary as to how the rupture process of Fault 2 is influenced by how the rupture on Fault 1 terminates. The rupture process of Fault 2, however, does not depend on specific elastic waves radiated from specific points, e.g. a stopping phase (Bernard & Madariaga 1984), but rather depends on stress perturbations caused by the overall rupture on Fault 1.

We also examined cases in which the upper edge of Fault 2 did not reach the Earth's surface. Our simulation shows that when a weak plane for Fault 2 reaches the Earth's surface, rupture is easily triggered on Fault 2. This is because the free surface, if Fault 2 reaches it, can efficiently decrease normal stress on Fault 2.

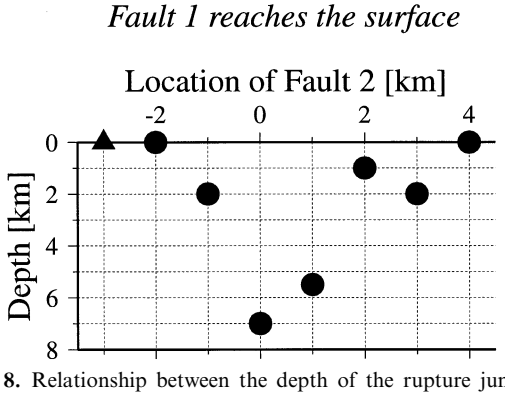

Figure 8. Relationship between the depth of the rupture jump and the horizontal location of Fault 2 in model B. Faults 1 and 2 reach the Earth's surface. The distance between Fault 1 and the edge of Fault 2 is 1.0 km. The edge of Fault 1 is located at $x = 0$. The horizontal axis is the location of Fault 2 given in the x-coordinate. The vertical axis is the depth of rupture jump. Circles mean that ruptures propagate on Fault 2. The triangle means that rupture is triggered but soon terminates.

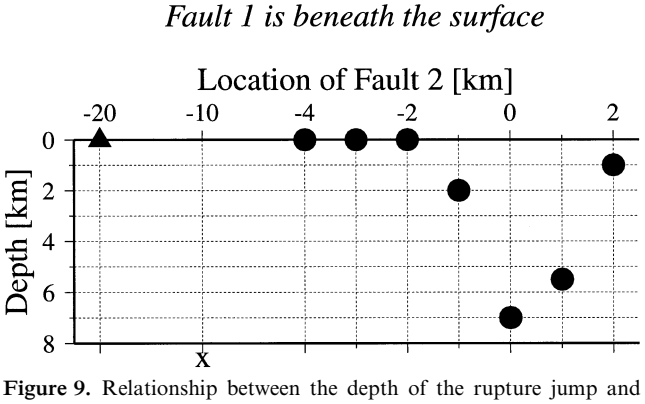

Figure 9. Relationship between the depth of the rupture jump and the horizontal location of Fault 2 in model B. Fault 1 does not reach the Earth's surface, but Fault 2 does. The distance between Fault 1 and the edge of Fault 2 is 1.0 km. The edge of Fault 1 is located at $x = 0$. Crosses indicate that rupture cannot be triggered on Fault 2. The other details are the same as for Fig. 8.

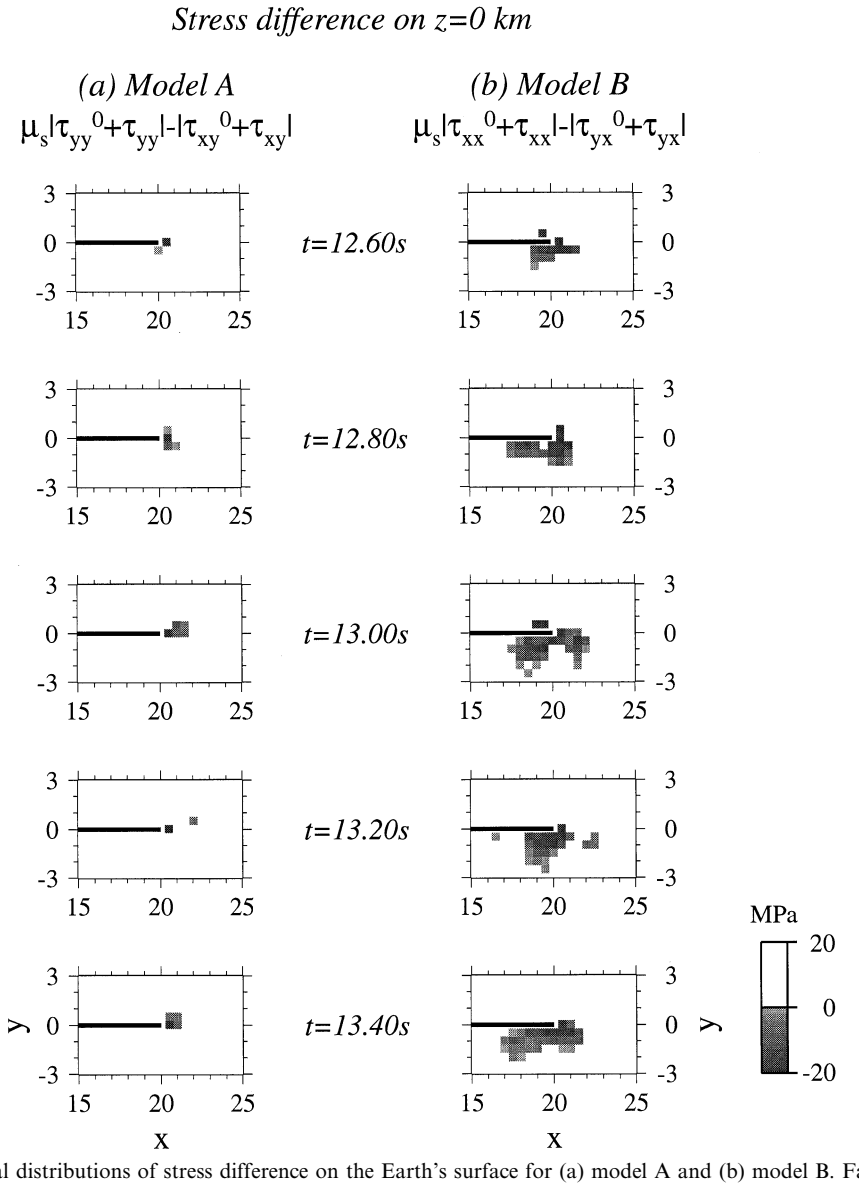

Figure 10. Spatio-temporal distributions of stress difference on the Earth's surface for (a) model A and (b) model B. Fault 1 reaches the Earth's surface. Solid lines indicate Fault 1. The negative values indicate that Fault 2, which is (a) parallel or (b) perpendicular to Fault 1, can rupture if it exists there.

4.2 Effect of fault strike and location

In model B, the relative locations of the two faults are very important in determining whether or not rupture can jump. Our results have shown that rupture can jump to Fault 2 only in a region where the normal stress generated by the rupture on Fault 1 is extensional (Fig. 7). In contrast, in model A, rupture can jump in both compressional and extensional cases.

The observations suggest that normal stress generated by rupture on Fault 1 more strongly controls the rupture jumps in model B than in model A. This difference is attributed to the different components of normal stress. The normal stress component is τ_{yy} in model A and τ_{xx} in model B. Since a stress perturbation caused by slip on Fault 1, Δu_x, is more influential in τ_{xx} than in τ_{yy}, the difference between compressional and extensional cases is clearer in model B than in model A.

The difference in the stress field between models A and B is observed in the spatio-temporal distribution of stress difference, $\Delta s(\boldsymbol{x}, t)$, as shown in Figs 10 and 11. Normal stress caused by the rupture on Fault 1 is compressional in $y>0$ and extensional in $y<0$. In model A, negative $\Delta s(\boldsymbol{x}, t)$ appears in the limited region near the edge of the fault, but exists on both the compressional and the extensional sides (Fig. 10a). In model B, the area of $y>0$ is almost completely characterized by positive values of $\Delta s(\boldsymbol{x}, t)$ (Figs 10b and 11b) so that rupture cannot jump to Fault 2 in that region. However, in $y<0$, there exists a significant region of negative $\Delta s(\boldsymbol{x}, t)$. The negative region is much larger in model B than in model A. Rupture can easily jump to Fault 2 in the extensional region if Fault 2 exists there. The rupture, however, cannot expand on Fault 2 immediately because the triggered point is located in the stress shadow of rupture propagating on Fault 1 and the shear stress concentration is suppressed. The rupture can start to propagate on Fault 2 when the rupture on Fault 1 completely terminates and the stress shadow of the rupture on Fault 1 starts to disappear.

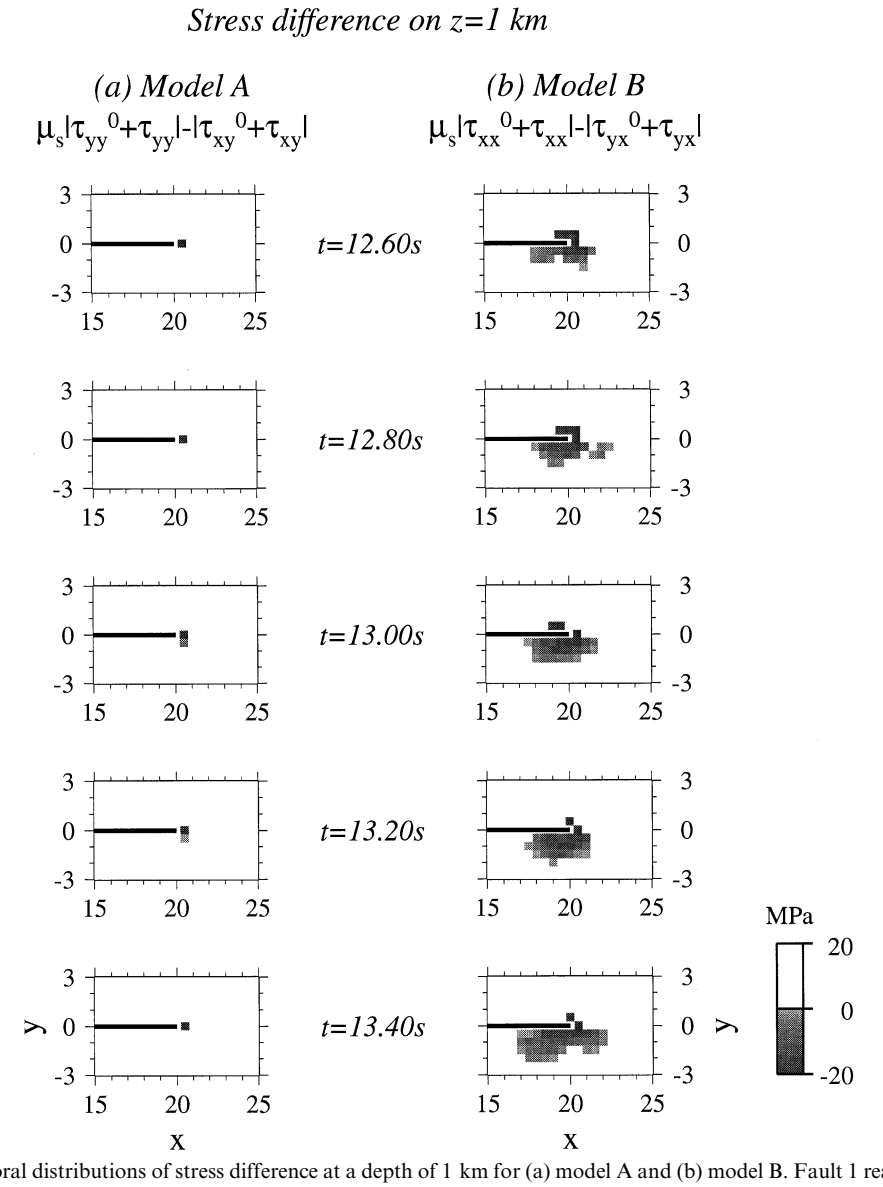

Figure 11. Spatio-temporal distributions of stress difference at a depth of 1 km for (a) model A and (b) model B. Fault 1 reaches the Earth's surface. The details are the same as for Fig. 10.

The depth variation of the rupture jump as shown in Fig. 8 can also be explained by considering normal stress and shear stress concentrations close to the edge of Fault 1. The effective strength of Fault 2 becomes small due to low normal stress. When Fault 2 is located very close to the edge of Fault 1, a small stress perturbation generated at the deep edge of Fault 1 can trigger rupture on Fault 2. When Fault 2 is located at a great distance from the edge of Fault 1, the stress perturbation around the deeper edge is too small to trigger rupture on Fault 2. Rupture is triggered on Fault 2 by a large stress perturbation at a shallow edge of Fault 1. Behind the edge of Fault 1, the concentration of shear stress is suppressed by rupture on Fault 1 when Fault 1 reaches the Earth's surface. Rupture can jump to Fault 2 only at a short distance from the edge of Fault 1.

When rupture on Fault 1 terminates beneath the Earth's surface and Fault 2 is located far from the edge of Fault 1, rupture on Fault 2 cannot be triggered or soon terminates in model B (Fig. 9). Since only a small portion of Fault 2 is located in a region of negative $\Delta s(\boldsymbol{x}, t)$ (Fig. 12b), it is difficult to induce catastrophic rupture on Fault 2. However, in model A, a large portion of parallel Fault 2 is located in a region of negative $\Delta s(\boldsymbol{x}, t)$ (Fig. 12a). The rupture propagates easily along the upper edge of Fault 1.

4.3 Effect of heterogeneity

Although we address the role of fault geometry in this paper, in this section we briefly demonstrate the effect of fault heterogeneity on rupture jumps, assuming that the strength of Fault 2 is smaller than that of Fault 1. This assumption can express situations in which the shear stress on Fault 2 is already high enough because of adhesion, situations in which the static frictional stress on Fault 2 is decreased by pore pressure, and situations in which the angle between the maximum compressional stress and Fault 1 is more obtuse than that between the maximum compressional stress and Fault 2 for model B.

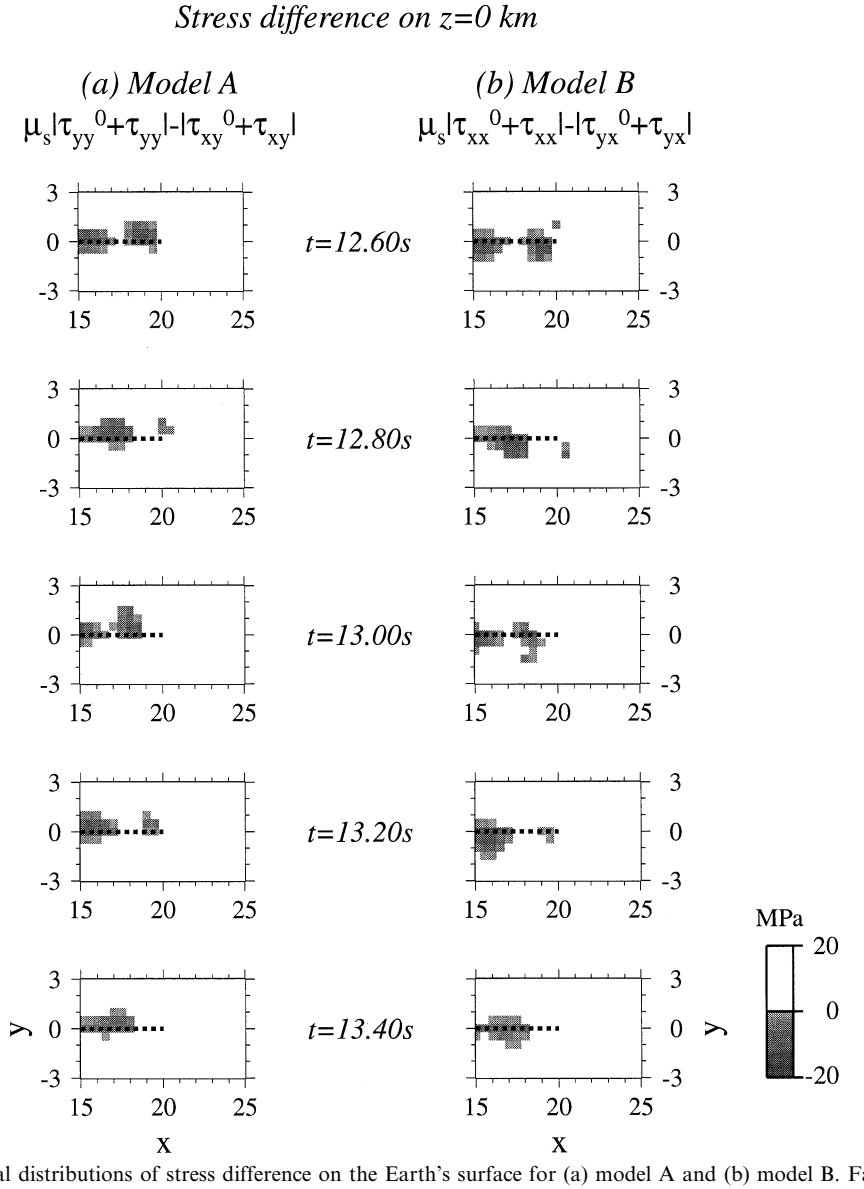

Figure 12. Spatio-temporal distributions of stress difference on the Earth's surface for (a) model A and (b) model B. Fault 1 does not reach the Earth's surface. Dotted lines indicate Fault 1 located at a depth of 1 km. The details are the same as for Fig. 10.

When the strength of Fault 2 is smaller than that of Fault 1, rupture is triggered at a deep part of Fault 2. Fig. 13 shows rupture evolution in model A when the strength of Fault 2 is less than that of Fault 1. In this case, we assume the smaller static coefficient of friction and the larger dynamic coefficient of friction for Fault 2 so that both the strength and the stress drop of Fault 2 are 34 per cent of those of Fault 1. The location of the rupture jump is different from that when the strengths of the two faults are the same (Fig. 5). We also see in model B that the depth of the rupture jump tends to be deeper as the strength of Fault 2 is weaker. In model B, rupture can jump only when Fault 2 is located in the region of extensional normal stress.

The difference in the depths of the rupture jump can be attributed to different magnitudes of stress perturbations generated at different depths. When the rupture arrives at an edge of Fault 1, a stress perturbation occurs around the edge. The magnitude of the stress perturbation is smaller at a deep edge of Fault 1 than at a shallow edge. When the strength of Fault 2 is small, rupture on Fault 2 can be initiated by a small stress perturbation around the deep edge of Fault 1. However, for a strong Fault 2, the stress perturbation is too small to rupture Fault 2. Rupture is not initiated on Fault 2 until a large stress perturbation occurs at a shallow edge.

The rupture pattern on weak Fault 2 is different from that of strong Fault 2 when comparing Figs 5 and 13. The rupture on weak Fault 2 cannot propagate towards a region where Fault 2 overlaps with Fault 1. When the rupture on Fault 1 terminates beneath the Earth's surface, rupture is additionally triggered at the upper edge of Fault 2, which is the same as Fig. 6(a), but the rupture cannot propagate downwards to a region where Fault 2 overlaps with Fault 1. These observations are similar to the 2-D simulations of Kase & Kuge (1998). In our simulation, the ratio between strength and stress drop (the *S*-value; Eq. 8) is assumed to be the same on the two faults. Less strength in

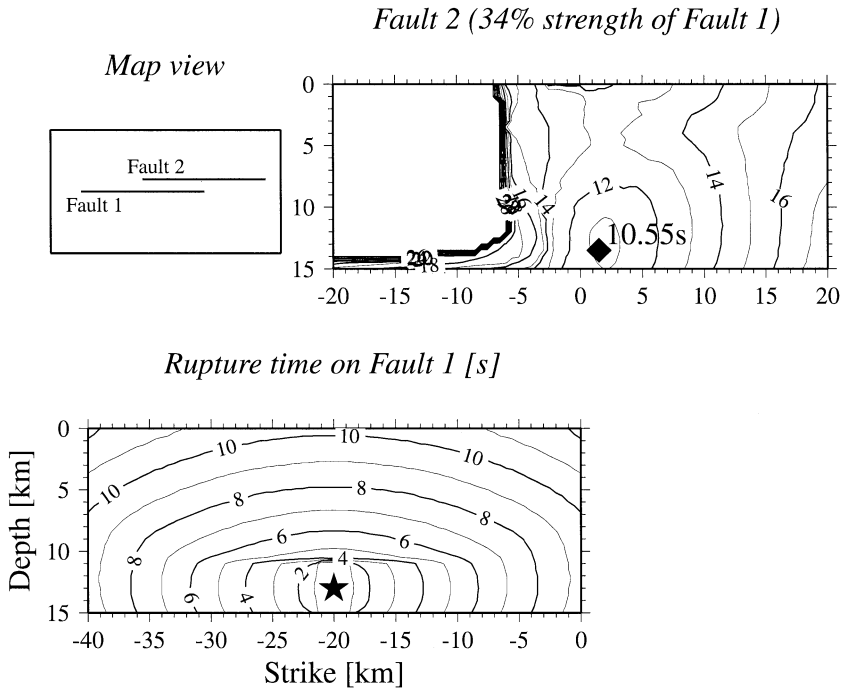

Figure 13. Rupture evolution on Faults 1 and 2 (compressional jog) in model A when the strength of Fault 2 is 34 per cent that of Fault 1. The two faults reach the Earth's surface. The details are the same as for Fig. 5.

Fault 2 involves a smaller stress drop. The small stress drop on Fault 2 prevents rupture from propagating towards the region where the rupture on Fault 1 suppresses stress.

Our results show that variations in strength and stress drop can provide an additional variety of rupture patterns on Fault 2. At the same time, it is implied that the depth of rupture jumps across stepovers can qualitatively indicate differences in strength between the two faults.

4.4 Implications for the Landers and Kagoshima earthquakes

Finally, based on our results, we discuss the rupture processes of two earthquakes, the 1992 Landers, California, earthquake and the May event of the 1997 Kagoshima, Japan, earthquake. The former and latter are examples of models A and B of our simulations, respectively.

In the 1992 Landers earthquake, excellent surface breaks were observed throughout the five faults (Fig. 1) (Sieh *et al.* 1993). The main rupture propagated on the Johnson Valley, Homestead Valley and Emerson faults, across at least two stepovers (e.g. Wald & Heaton 1994; Aydin & Du 1995). Rupture started at the centre of the southernmost Johnson Valley fault. Rupture expanded unilaterally north- to northwestwards. The distance between the faults in the stepovers was a few kilometres. The fault segments were extensional jogs in vertical strike-slip faults. Wald & Heaton (1994), who determined the rupture evolution by modelling the strong-motion and teleseismic waveforms and geodetic deformations, suggested that the rupture decelerated near the stepovers and estimated that the large dislocations were at the shallow parts of the faults. The surface offsets were also large near the stepovers (Aydin & Du 1995).

Our simulations have shown that rupture can jump beyond a stepover at the Earth's surface on faults intersecting with the Earth's surface. It is likely for the 1992 Landers earthquake that the large dislocations at the shallow parts caused large stress perturbations at shallow depths and led to rupture propagation beyond the stepovers.

The May event of the 1997 Kagoshima earthquake consists of two conjugate strike-slip faults (Fig. 2), which is suggested from the distribution of the aftershocks (e.g. Miyamachi *et al.* 1999) and the rupture models obtained from the strong-motion waveforms (e.g. Miyake *et al.* 1999; Horikawa 2001). One fault extends to the east and the other extends to the south. The precise location of the hypocentre tends to vary, depending on the researchers. It is clear, however, that the hypocentre was located near the junction of the two faults. The time lag of the ruptures on the two faults was estimated to be 1.0 s by Horikawa (2001) and 2.0 s by Miyake *et al.* (1999). The depth of the hypocentre is about 8 km (Faculty of Science Kagoshima University 1997). Since there are no observations of surface breaks for the Kagoshima earthquake, the two faults were embedded beneath the Earth's surface. The focal mechanism of the May event is characterized by almost pure strike-slip on vertical faults (Faculty of Science Kagoshima University 1997), which involves a left-lateral slip on the east–west-striking fault and a right-lateral slip on the north–south-striking fault. Therefore, normal stress caused by rupture on one fault was extensional on the other fault.

Our simulations have shown that rupture easily jumps to perpendicular Fault 2 when the normal stress caused by rupture on Fault 1 is extensional. The fault geometry of the May event agrees with this result. In our simulation for Fault 2 with the same strength as Fault 1, however, rupture could not propagate to Fault 2 when the upper edges of the two faults are beneath the Earth's surface. The rupture jumped at the shallow

portion less than 1 s after the rupture on Fault 1 arrived at the fault edge, but terminated shortly afterwards. Moreover, Horikawa (2001) suggested that the rupture of the May event jumped at the deep portion near the hypocentre with a time delay of 1.0 s. We cannot deny that, given the constraint of his source inversion, rupture is forced to propagate smoothly, possibly causing rupture on the second fault to start near the hypocentre. However, as shown in the previous section, fault heterogeneity is one interpretation accounting for the difference between the rupture process of this earthquake and our numerical simulation. The strength could be very weak in the region where the rupture jumped. Alternatively, there could be a connection between the two conjugate faults, at least near the hypocentre, which was not considered in our simulations.

5 CONCLUSIONS

We carried out 3-D numerical simulations using two non-coplanar strike-slip faults. We found that rupture processes across fault discontinuities are influenced by three factors:

(i) depth of the upper edge of the two faults, especially whether the faults reach the Earth's surface or not;
(ii) location of the edge of the first fault;
(iii) geometry (e.g. strike and step direction) of the two faults.

These factors affect when and where rupture is triggered and how rupture propagates on the second fault.

Most of the successful rupture jumps in our numerical simulations occur very close to the Earth's surface. The exceptions are the limited cases when the two faults are perpendicular. Moreover, we have found that whether rupture on the first fault reaches the Earth's surface or not controls not only the degree of difficulty but also the locations of rupture jumps, relating to the step direction of the two faults. The Earth's surface thus has a strong influence on rupture processes across fault discontinuities.

ACKNOWLEDGMENTS

We thank Steven M. Day and Ruth A. Harris for their helpful suggestions. We also thank Tomotaka Iwata, Mamoru Kato, Shin Aoi, Haruo Horikawa and Takane Hori for their useful discussions. H. Horikawa gave us the fault model of the 1997 Kagoshima earthquake. We thank R. A. Harris and Shamita Das for their thoughtful reviews. YK was supported by Research Fellowships of the Japan Society for the Promotion of Science for Young Scientists. We used GMT [Generic Mapping Tool version 3.1.1; Wessel & Smith (1995)] for drawing some figures.

REFERENCES

Aki, K., 1979. Characterization of barriers on an earthquake fault, *J. geophys. Res.,* **84,** 6140–6148.

Andrews, D.J., 1976. Rupture velocity of plane strain shear cracks, *J. geophys. Res.,* **81,** 5679–5687.

Antonioli, A., Cocco, M., Das, S. & Henry, C., 2000. Dynamic stress triggering during the great March 25, 1998, Antarctic Plate (M_w8.1) earthquake, *EOS, Trans. Am. geophys. Un.,* **81,** F1199.

Aydin, A. & Du, Y., 1995. Surface rupture at a fault bend: the 28 June 1992 Landers, California, earthquake, *Bull. seism. Soc. Am.,* **85,** 111–128.

Bernard, P. & Madariaga, R., 1984. A new asymptotic method for the modeling of near-field accelerograms, *Bull. seism. Soc. Am.,* **74,** 539–557.

Das, S. & Aki, K., 1977. A numerical study of two-dimensional spontaneous rupture propagation, *Geophys. J. R. astr. Soc.,* **50,** 643–668.

Day, S.M., 1982. Three-dimensional simulation of spontaneous rupture: the effect of nonuniform prestress, *Bull. seism. Soc. Am.,* **72,** 1881–1902.

Faculty of Science Kagoshima University, 1997. The earthquakes with M6.3 (March 26, 1997) and with M6.2 (May 13, 1997) occurred in Northwestern Kagoshima Prefecture, *Rept Coordinating Committee for Earthquake Prediction,* **58,** 630–637.

Harris, R.A. & Day, S.M., 1993. Dynamics of fault interaction: parallel strike-slip faults, *J. geophys. Res.,* **98,** 4461–4472.

Harris, R.A. & Day, S.M., 1999. Dynamic 3D simulations of earthquakes on en echelon faults, *Geophys. Res. Lett.,* **26,** 2089–2092.

Harris, R.A., Archuleta, R.J. & Day, S.M., 1991. Fault steps and the dynamic rupture process: 2-D numerical simulations of a spontaneously propagating shear fracture, *Geophys. Res. Lett.,* **18,** 893–896.

Hart, E.W., Bryant, W.A. & Treiman, J.A., 1993. Surface faulting associated with the June 1992 Landers earthquake, California, *Calif. Geol.,* **46,** 10–16.

Henry, C., Das, S. & Woodhouse, J.H., 2000. The great March 25, 1998, Antarctic Plate earthquake: moment tensor and rupture history, *J. geophys. Res.,* **105,** 16 097–16 118.

Higdon, R.L., 1991. Absorbing boundary conditions for elastic waves, *Geophysics,* **56,** 231–241.

Horikawa, H., 1996. Inversion for dynamic source parameters: application to the 1990 Izu-Oshima, Japan, earthquake, *DSc thesis,* Kyoto University, Kyoto.

Horikawa, H., 2001. Earthquake doublet in Kagoshima, Japan: rupture of asperities in a stress shadow, *Bull. seism. Soc. Am.,* **91,** 112–127.

Ilan, A. & Loewenthal, D., 1976. Instability of finite difference schemes due to boundary conditions in elastic media, *Geophys. Prospect.,* **24,** 431–453.

Kame, N. & Yamashita, T., 1997. Dynamic nucleation process of shallow earthquake faulting in a fault zone, *Geophys. J. Int.,* **128,** 204–216.

Kase, Y. & Kuge, K., 1998. Numerical simulation of spontaneous rupture processes on two non-coplanar faults: the effect of geometry on fault interaction, *Geophys. J. Int.,* **135,** 911–922.

King, G. & Nábělek, J., 1985. Role of fault bends in the initiation and termination of earthquake rupture, *Science,* **228,** 984–987.

Kuge, K., Kikuchi, M. & Yamanaka, Y., 1999. Non-double-couple moment tensor of the March 25, 1998, Antarctic earthquake: composite rupture of strike-slip and normal faults, *Geophys. Res. Lett.,* **26,** 3401–3404.

Lindh, A.G. & Boore, D.M., 1981. Control of rupture by fault geometry during the 1966 Parkfield earthquake, *Bull. seism. Soc. Am.,* **71,** 95–116.

Magistrale, H. & Day, S.M., 1999. 3D simulations of multi-segment thrust fault rupture, *Geophys. Res. Lett.,* **26,** 2093–2096.

Mikumo, T., Hirahara, K. & Miyatake, T., 1987. Dynamical fault rupture processes in heterogeneous media, *Tectonophysics,* **144,** 19–36.

Miyake, H., Iwata, T. & Irikura, K., 1999. Strong ground motion simulation and source modeling of the Kagoshima-ken hokuseibu earthquakes of March 26 (M_{JMA} 6.5) and May 13 (M_{JMA} 6.3), 1997, using empirical Green's function method, *Zisin 2,* **51,** 431–442 (in Japanese with English Abstract).

Miyamachi, H., Iwakiri, K., Yakiwara, H., Goto, K. & Kakuta, T., 1999. Fine structure of aftershock distribution of the 1997 Northwestern Kagoshima Earthquakes with a three-dimensional velocity model, *Earth Planets Space,* **51,** 233–246.

Nettles, M., Wallace, T.C. & Beck, S.L., 1999. The March 25, 1998 Antarctic plate earthquake, *Geophys. Res. Lett.,* **26,** 2097–2100.

Quin, H., 1990. Dynamic stress drop and rupture dynamics of the October 15, 1997 Imperial Valley, California, earthquake, *Tectonophysics,* **175,** 93–117.

Scholz, C.H., 1990. *The Mechanics of Earthquakes and Faulting,* Cambridge University Press, Cambridge.

Sibson, R.H., 1985. Stopping of earthquake ruptures at dilational fault jogs, *Nature,* **316,** 248–251.

Sibson, R.H., 1986. Rupture interaction with fault jogs, in *Earthquake Source Mechanics*, eds Das, S., Boatwright, J. & Scholz, C.H., *AGU Geophys. Monogr.*, **37,** *Maurice Ewing Ser. 6*, 157–167.

Sieh, K., *et al.*, 1993. Near-field investigations of the Landers earthquake sequence, April to July 1992, *Science,* **260,** 171–176.

Wald, D.J. & Heaton, T.H., 1994. Spatial and temporal distribution of slip for the 1992 Landers, California, earthquake, *Bull. seism. Soc. Am.,* **84,** 668–691.

Wessel, P. & Smith, W.H.F., 1995. New version of the Generic Mapping Tools released, *EOS, Trans. Am. geophys. Un.,* **76,** 329.

Yamashita, T. & Umeda, Y., 1994. Earthquake rupture complexity due to dynamic nucleation and interaction of subsidiary faults, *Pure appl. Geophys.,* **143,** 89–116.